Delamination link-ups in composite laminates due to multiple hail impacts

Sadighi, Mojtaba; Alderliesten, René; Fathi, Azadeh; Soltannia, Babak; Hedayati, Reza

Important note
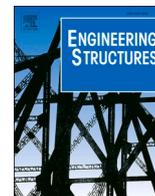To cite this publication, please use the final published version (if applicable).
Please check the document version above.

Delamination link-ups in composite laminates due to multiple hail impacts

Mojtaba Sadighi [a], René Alderliesten [b], Azadeh Fathi [a,c], Babak Soltannia [d], Reza Hedayati [e,*]

[a] *Department of Mechanical Engineering, Amirkabir University of Technology, P.O. Box 15875-4413, Tehran, Iran*
[b] *Structural Integrity & Composites Group, Faculty of Aerospace Engineering, Delft University of Technology, Netherlands*
[c] *Department of Human Centered Design, College of Human Ecology, Cornell University, Ithaca, NY, USA*
[d] *Department of Mechanical Engineering, University of Alberta, Donadeo Innovation Centre for Engineering, 9211-116 Street, NW, Edmonton, Alberta T6G 1H9, Canada*
[e] *Aerospace Materials and Structures (ASM) Department, Faculty of Aerospace Engineering, Delft University of Technology, Netherlands*

ARTICLE INFO

ABSTRACT

Damages to aircraft fuselages by ice impactors are categorized as barely visible impact damage (BVID). As the application of composite laminates in manufacturing aircraft fuselage is increasing rapidly, studying hail impact on composite laminates seems crucial. Investigation of variation of delamination area and link-up area for different impact scenarios between ice and carbon fibre prepreg composite plates is the main goal of this study. Link-up refers to joining of delaminated areas created by separate impacts at relatively close impact locations. To this aim, multiple impacts at 1 and up to 6 impact locations and with different impactor energies were simulated using SPH formulation, and delamination areas were quantified. The results showed that as the spacing L between two impact locations increases from 0 to $4R$ (where R denotes the impactor radius), the total delamination area first shows an increase up to a peak point (usually at $R < L < 2R$) after which it shows a large drop, and after $L \approx 2R$, the total delamination area level remains almost constant. The large drop is related to disappearance of the link-up phenomenon beyond a certain spacing. Moreover, it was observed that increasing the number of impact locations increases the delamination area almost linearly. As for the impactor energy influence, the results showed that as the impact energy increases, the threshold spacing for link-up increases. Moreover, for the case of impact at two locations and constant total energy level, two impactors with identical energy level lead to higher delamination area as compared to impactors with non-identical energy levels.

1. Introduction

Hail and bird impacts are known to be among the most concerning foreign object damages (FOD) to jet engines and leading edge structures [1–3]. As compared to hail impact, bird impact has a more serious effect on the proper performance of the aircraft. However, unlike hail damages, the damages caused by bird impacts are usually easily detectable due to their high severity [4]. Damages due to ice impactors are categorized as barely visible impact damage (BVID) [5], even though in some cases it can even lead to dents and perforations [6]. The wing and tail leading edges of airplanes are not the primary damage concerns for hail impacts as they are usually designed to be resistant against bird strike and also due to the fact that they are easily separable from the main fuselage for repair and replacement. The top surfaces of fuselage, wings, and tailplanes are, however, still under-designed for free-fall (~45 m/s [7]) hail impacts when the airplane is parked on the ground. The hail velocity can be increased even further by wind of different directions and velocities [8], which has an exponential effect on the kinetic energy sustained by the impacted structure. Special results of COVID-19 pandemic in the form of long-term parking of airplanes in open spaces increased the attention to ice impacts even further [9]. Recent research has shown that global warming can increase the kinetic energy of hailstorms by 40% by 2040 [5,10].

Most of the previous research works on hail impact has been performed on metal (e.g. aluminum [6,11] and steel [12,13]) fuselage [14]. As the application of composite laminates in manufacturing aircraft fuselage is increasing rapidly, the need to study hail impact on composite laminates seems crucial. While being advantageous in mechanical and weight aspects, composite plates show much more complexity in their impact response. The first work on simulation of ice impact on composite structures was performed by Kim and Kedward [15] who studied the impact resistance of carbon/epoxy composite in high velocity regime (30–200 m/s) using numerical and experimental approaches. Appleby-Thomas et al. [16] investigated ice impacts with

* Corresponding author.
E-mail addresses: r.hedayati@tudelft.nl, rezahedayati@gmail.com (R. Hedayati).

carbon-fibre reinforced composites (CFRCs) for impact energies in the range of 72–1215 J. They observed that sub-surface disruption and residual compressive strength both have linear relationship with impact energy, suggesting the occurrence of cumulative damage in such structures. In later studies, several types of woven [17] and UD tape prepeg [18,19] carbon/epoxy composites were studied as well. Dolati et al. [20] investigated the impact resistance of glass-fibre epoxy laminates with different stacking sequences including 0/90, ±45, chopped strand mat (CSM), and unidirectional fibre orientations. They reported the plain weave 0/90 lay-up to be the most susceptible case to damage. The advantages of inclusion of ± 45 plies in the laminate in improving the impact resistance has been reported in other works as well [21].

Several material models have been proposed and studied for simulating ice behavior at high strain rates. Kim and Kuene obtained compressive strength of ice in high strain rates [22]. Tippman et al. [23] used those data to develop a strain rate dependent material model for ice. In their model, a tensile pressure criterion could be activated when the hydrostatic tensile stress reached a critical value. Carney et al. [24] developed a phenomenological model for ice taking into account strain rate effects, which had the ability to allow ice to continue to carry hydrostatic stress after failure. Chuzel et al. [25] implemented an isotropic damage model for concrete which assumes exponential softening behaviour and includes independent damage variables in compression and tension. Several numerical techniques such as Lagrangian, Arbitrary Lagrangian Eulerian (ALE), and Smoothed Particles Hydrodynamics (SPH) have been previously used to model ice impact onto rigid and deformable plates. SPH has proven to be the most accurate and the most efficient formulation among the three [6].

Composite plates fail due to several factors: cracks along the fibres, fibre fracture, and delamination between plies [18–21,26–30,67]. Among the three noted failure mechanisms, delamination accounts for more than 60% of total failure modes [31]. As compared to other foreign object impactors, ice impacts are unusual as they can cause several impacts at one or multiple locations [16]. A single impact on a composite component may not result in any tangible damage, but the damage accumulation caused by multiple or repeated impacts may significantly increase the probability of reducing load bearing capacity, and therefore, the likelihood of unexpected failures. Despite the presence of extensive number of studies dealing with single low-velocity impacts [32], only a limited number of studies have been conducted on repeated impacts or multiple impacts on composite structures [33]. Furthermore, despite the presence of a number of experimental and numerical works on the hail impacts on composite plates, parametric studies on the effect of number of impacts on the delamination area and link-up region is still lacking. Link-up refers to joining of delaminated areas in a composite plate resulted from separate impacts at different but relatively close impact locations. The effects of varying the impactor's energy as well as increasing asymmetry in the energy level of different impactors while keeping the total incoming energy level constant are other areas of research which require attention.

In this paper, a numerical model is presented to simulate the impact between ice and carbon fibre prepeg composite plates. The objective is to investigate how the delamination areas and their link-up characteristics vary for different impact scenarios. To this aim, a mesh-less SPH formulation is implemented for modelling the ice impactors in LS-DYNA, while the composite target plate is modelled using Lagrangian technique. To vary impact scenarios, multiple impacts at one up to 6 impact locations are simulated, and delamination areas are quantified. Moreover, the impactor energy, the spacing between the impact locations, and the number of impact locations are varied and their effects on delamination area are studied.

2. Materials and methods

2.1. Modelling of ice

The SPH method has previously been used for modelling ice impactors [34]. Under high velocities, the ice behaves like a fluid projectile which can be modelled using the SPH elements. SPH is a mesh-less FE method based on Lagrange formulation where the material is represented by discrete particles interacting with each other. The SPH method was first introduced in 1970s [35,36] for astrophysics problems, but in the decades after, it found its way into solving transient fluid flow problems. It uses interpolation of compact support to represent any field quantity as a set of discretized particles. The interpolation kernel determines the contribution of neighboring particles in the properties of a point of interest [3]. As this method does not require a computational mesh, the SPH interpolation uses a smooth weighting function (kernel) and the particle position to estimate the variable gradients for a range of parameters. For a particle i, the value of arbitrary function F is approximated by

$$\langle F_i \rangle = \sum_j V_j F_j W_{ij} \tag{1}$$

where $V_j = \frac{m_j}{\rho_j}$ is the fluid volume assigned to each particle, and $W_{ij} = W_h(r_i - r_j, h)$ is a smooth kernel function with h representing its smoothing length, by which the area of area of W (the radius of its support domain) is defined. As indicated in Fig. 1, a property's value at a point of interest is determined by summing the values of the property at the neighboring particles, weighted by the kernel function. In this research, the SPH ice impactor was composed of 2,176 elements with a spacing of 1.8 mm.

2.2. Geometry

To simulate the effect of impact spacing on the damage response of the laminate, the explicit LS-DYNA V11.1 FE code was implemented. Fig. 2 shows the FE model of SPH hail and the composite target with the stacking sequence of [45,0,−45,90,45,0,−45,90]$_s$. This layup was chosen due to the stacking sequence recommended in the ASTM D7136/D7136M [37]. Furthermore, the layup was chosen as a quasi-isotropic, symmetric, and balanced stacking sequence based on the complex and large number of load cases that the fuselage must be able to endure [38]. The dimensions of the target plate and impactor are given in Table 1. To evaluate the mesh independency, a mesh sensitivity analysis was conducted by reducing the size of the element from 4 mm to 0.5 mm. The convergence was obtained with 1 mm element size. Therefore, the total number of elements of a composite ply was measured to be 51,000. The diameter of 0.5 cm is usually taken as the threshold dimension for
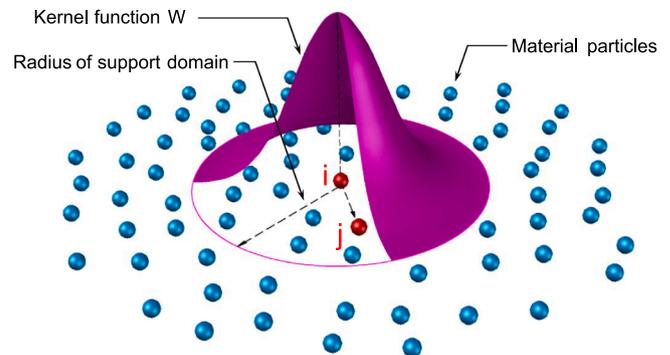

Fig. 1. An illustration of how the SPH method uses field variables approximation for the properties of a particle of interest *i* interacting with a neighboring particle *j* within the support domain of the smoothing kernel function *W*.
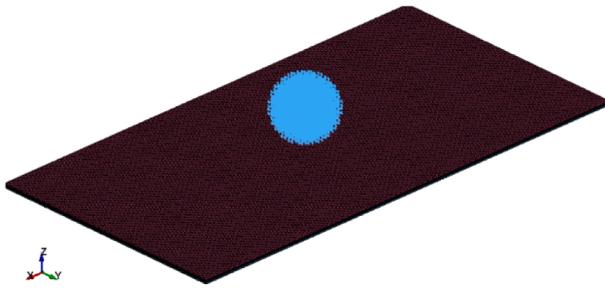
Fig. 2. Finite element model of the laminate and hail impactor.

Table 1
The geometrical parameters of the target plate and impactor.

Parameter	Value
Laminate dimension	215 mm × 120 mm
Laminate thickness	2.5 mm
Ply thickness	0.156 mm
Hail diameter	30 mm

transitioning between graupel and hail [39]. According to an analysis [40] on the European severe weather database (ESWD), maximum hail dimension is in the range of 20–29 mm. In particular circumstances such as the hail storm in Dallas USA, ice sizes as large as 10 cm have been reported which caused damage to more than 100 aircrafts parked outdoors [20,41]. Nonetheless, in this research, an ice impactor of 30-mm diameter has been considered for the simulations.

For perfect spheres under ideal falling conditions, the terminal velocity can be found using $V_{Ter} = \sqrt{\frac{2mg}{\rho A C_D}}$ where m, ρ, and A respectively represent the mass, density, and area of the ice projectile, g stands for the gravitational constant (9.81 m/s^2), and C_D represents the drag coefficient. For the considered ice diameter of 30 mm, the terminal velocity is obtained to be 26.5 m/s. The initial velocity of the ice impactor was set to 30 m/s. The considered difference between the set initial velocity and the calculated terminal velocity is due to the fact that, in most experimental and numerical studies, it is desirable to propel the ice spheres slightly above the magnitude of the terminal velocity due to environmental effects such as wind [8]. The plate was fully constrained (against motion in the X, Y, and Z directions, as well as rotations about the same axes) at its boundaries.

2.3. Material and contact modeling

LS-DYNA offers several material models for composite materials. In this research, *MAT_ENHANCED_COMPOSITE_DAMAGE (Material number 054/055) was selected for modelling the material behavior of composite plies. The material model MAT 054 uses Chang-Chang failure criteria and has an orthotropic progressive failure, which makes it an ideal model for unidirectional fibers. In tension, compression, and shear, the model acts in a linear elastic manner until the element's developed stresses reach the yield strengths. In this failure criteria, in addition to tensile and compressive fiber failure, matrix failure mode is also considered. Failure occurs when one of the following failure criteria is met. The fibers fail when:

$$e_f^2 = \left(\frac{\sigma_{11}}{S_{XL}}\right)^2 + \beta\left(\frac{\sigma_{12}}{S_s}\right) - 1 \geq 0 \qquad (2)$$

where σ_{11} and σ_{12} are the normal and shear stresses, S_L is the longitudinal strength ($S_L = S_t$ in tension and $S_L = S_c$ in compression), S_s is the shear strength, and β is the weighting factor for shear term in tensile fiber mode β enables the user to explicitly define the effect of shear in the tensile fiber mode. This value ranges from 0 to 1.0, and the Hashin fiber

tension criterion is applied when $\beta = 1$. When $\beta = 0$, Equation (2) is reduced to the Maximum Stress failure criterion, which is the only alteration to the original Hashin failure criterion in MAT 054. Choosing the β value is a matter of preference that can be determined by trial and error [42]. The $\beta = 0$ value is considered appropriate for materials showing brittle behavior [43]. Considering the suggestions in the literature and after conducting some parametric studies, $\beta = 0$ was observed to provide a good agreement with the experimental data.

The matrix fails under tensile stress when:

$$e_m^2 = \left(\frac{\sigma_{11}}{S_{Yt}}\right)^2 + \left(\frac{\sigma_{12}}{S_c}\right)^2 - 1 \geq 0 \qquad (3)$$

and fails in compression when

$$e_d^2 = \left(\frac{\sigma_{22}}{2S_c}\right)^2 + \left[\left(\frac{S_{Yc}}{2S_c}\right)^2 - 1\right]\frac{\sigma_{22}}{S_{Yc}} + \left(\frac{\sigma_{12}}{S_c}\right)^2 - 1 \geq 0 \qquad (4)$$

In the above equations, S_{Yt} is the transverse tensile strength and S_{Yc} is the transverse compressive strength. The material properties of the composite laminate are listed in Table 2.

To model the hail impactor, *MAT_PLASTICITY_COMPRESSION_TENSION_EOS (Mat 155 in LS-DYNA) and *EOS_TABULATED_COMPACTION were used as the material model and equation of states, respectively. The input values of the material are reported in Table 3. The equation of state (EOS) relates the volumetric strain and pressure in the ice impactor material and its values are listed in Table 4 and demonstrated in Fig. 3a. Additionally, the effect of strain rate on material behavior was considered in the model in accordance with results of [24] (see Fig. 3b).

Contact type AUTOMATIC_NODES_TO_SURFACE in LS-DYNA was defined between the ice impactor and the target plate. In cases where the elastic bulk moduli of the parts in contact are widely different from one another, a soft constraint can be beneficial. Using the soft constraint option in contact, the interface stiffness is determined by the nodal mass and the global time step size. Therefore, the "SOFT 1″ formulation was activated, resulting in better interaction between the soft impactor and relatively stiff target.

Additionally, to take the delamination between the layers into account, contact type AUTOMATIC-SURFACE-TO-SURFACE-TIEBREAK was defined between the layers. The tiebreak option enabled the contact surfaces to be detached after reaching maximum normal stress (NFLS) or shear stress (SFLS). The delamination area was visualized using INTFOR option in LS-DYNA.

In the repeated impact simulations, the impactors were positioned at specific distances from each other on a straight line, impacting the panel one after another. As a result of the initial impacts, some permanent delamination was induced in the panels which remained until the next impactor impacted the same position. The damage accumulation in the laminates gradually increased as a result of each consecutive impact.

It must be noted that throughout the rest of the paper, we use the term *delamination area* to refer to total accumulated delamination area in each composite laminate caused by all impactors and at different instances.

Table 2
Material properties of composite laminate [38].

Parameter	Description	Value
E_A	Young's modulus - Longitudinal	145 GPa
E_B	Young's modulus - Transverse	8.1 GPa
G_{AB}	Shear modulus – AB plane	3.4 GPa
X_C	Compressive strength – Longitudinal	1020 MPA
X_T	Tensile strength – Longitudinal	3010 MPa
Y_C	Compressive strength - Transverse	138 MPa
Y_T	Tensile strength - Transverse	39 MPa
S_C	Shear strength - AB plane	95.6 MPa

Table 3
Material properties of hail [24].

Parameter	Value
Diameter	30 mm
Density	897 kg/m3
Young's modulus	9.31 GPa
Poisson's ratio	0.33
Pressure cut-off in tension	0.433 MPa
Pressure cut-off in compression	4.93 MPa

Table 4
Equation of State loading table for ice [24].

Volumetric strain	Pressure	Bulk modulus
0	0 MPa	8.96 GPa
-7.69×10^{-3}	68.9 MPa	8.96 GPa
-3.13×10^{-2}	68.9 MPa	2.2 GPa
-10	68.9 MPa	6.89 MPa

3. Results

3.1. Validation of the model

With the goal of validating the numerical model of the hail impactor, a finite element (FE) model of the hail impactor and rigid target plate was constructed, and the results were compared with those obtained from experimental investigation undertaken by Carney et al. [24]. The cylindrical hail impactor had a diameter of 17.5 mm and a length of 42 mm. The rigid target plate was a circular steel plate with a diameter of 63.5 mm and a thickness of 19 mm. The experimental and numerical results are compared in Fig. 4 which illustrate good agreement between the experimental data and the numerical predictions.
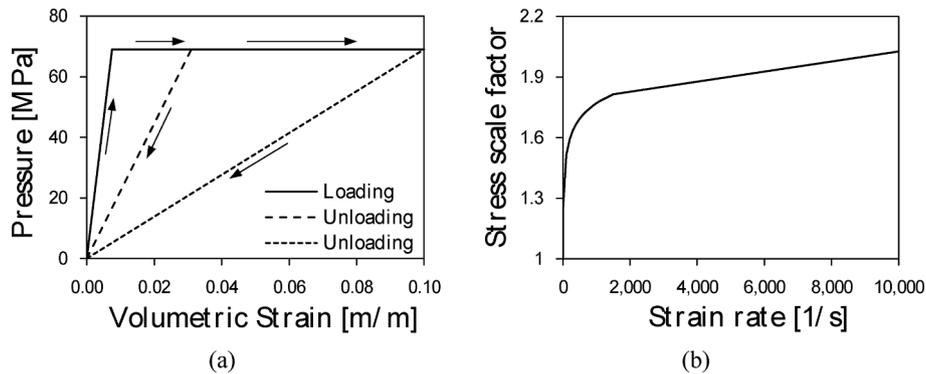
To confirm the reliability and accuracy of the numerical analysis in modelling the hail impactor with deformable composite plate, the FE models were validated against the experimental result [38]. To investigate the effect of impact spacing on the damage response, the specimens were impacted at three locations on the plate. As depicted in Fig. 5 (a, b) impacts were spaced at the $L = 2R$ and $L = R$. Each location was impacted 5 times and the energy of the impactor was set to 6 J.

Fig. 5c-f compares the numerical/experimental delamination areas of the composite laminate. The experimental delamination areas were obtained using C-scan method in [38] for steel impactors. To validate the behavior of the composite plate, steel impactor having the initial kinetic energy of 6 J was considered for the validation simulations. The composite panel was subjected to 5 impacts per location (5IPL) at three specified locations. The impactor had a mass of $0.165kg$ and an initial velocity of $v = 8.6m/s$. The simulations with steel impactor were carried out to evaluate the accuracy of the composite plate and contact modelling. Fig. 5 demonstrates a good agreement between the numerical on the one hand and experimental results on the other hand. The maximum difference between the numerical and experimental delamination areas was $< 6\%$. After the numerical model was validated, different impact scenarios were studied using ice impactors the results of which are presented in the next subsections.

3.2. Single location impact response

Fig. 6 demonstrates the deformation of the hail impactor with kinetic energy of 6 J at different time instances. The partial failure of the hail in contact with the composite panel at the beginning (Fig. 6b), the expansion of contact area (Fig. 6c,d), and finally, the complete flattening of the remaining hail impactors can be seen in this figure. This is in accordance with experimental observations that have shown fluid-like behavior of the ice impactor in high impact velocities (see Fig. 7 in [14]).

Fig. 3. (a) Equation of state relating pressure and volumetric strain in both loading and unloading regimes [24], and (b) stress scale factor due to strain rate effect [24].
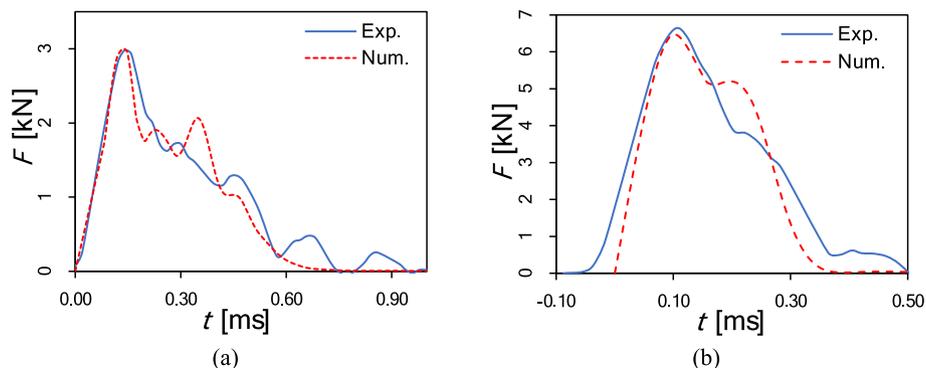

Fig. 4. Comparison of the numerical and experimental [24] results of the hail impact on rigid plate with impactor's initial velocity of: (a) 91 m/s and (b) 152 m/s.
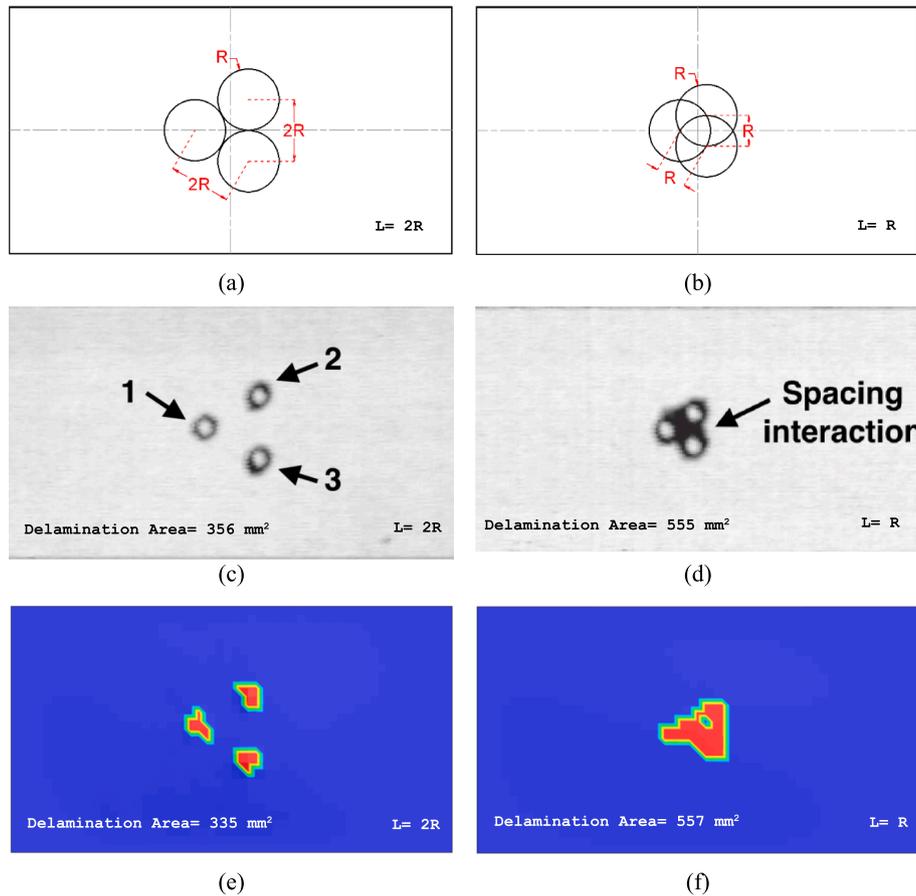
Fig. 5. Comparison of delamination area: (a,b) schematic of impact locations, (c,d) experimental results [38], and (e,f) numerical results from the steel impactor. The left and right columns present the results for $L = 2R$ and $L = R$, respectively.
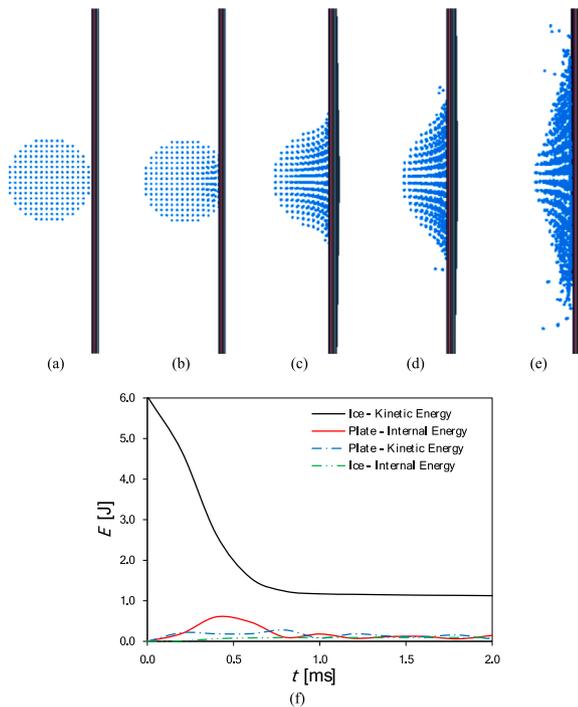

Fig. 6. The deformation of a hail impactor with kinetic energy of 6 J at (a) 0 ms, (b) 0.1 ms, (c) 0.4 ms, (d) 0.6 ms, and (e) 1 ms. (f) Variation of energy level of the ice impactor and composite plate for the same impactor.

As it can be seen in Fig. 6f, before hitting the target plate, the system's energy is in the form of kinetic energy of the ice impactor only. As soon as the impact occurs, the initial impactor's kinetic energy starts dissipating due to deformation in the ice impactor and the target plate as well as damage initiation and propagation in the composite laminate. Moreover, the kinetic energy starts converting into internal energy in the target plate and the ice impactor. As it can be seen in Fig. 6f, during the impact, the kinetic energy of the ice impactor decreases while the laminate's internal energy rises. The laminate's internal energy peaks at
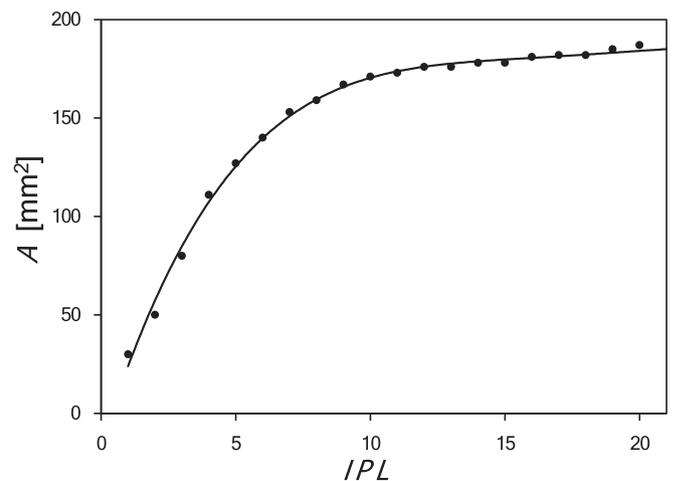

Fig. 7. Variation of delamination area with respect to the number of impacts per location (for impactor energy of 6 J impacting one location).

~ 0.4 ms which is the instance when the plate goes momentarily to rest. After that, when the composite laminate bounces back, a major portion of the stored energy is releases and hence the internal energy decreases. The results also show that the sliding and hourglass energy levels were quite low (<15%). It is worth noting that among all energies, the plate's kinetic energy as well as the internal energy of the ice impactor are relatively low. At its peak, the internal energy in the composite plate reaches 7.8% of the impactor's initial kinetic energy.

The question that might arise here is what would happen if the number of impacts in the single location increases. The results show that as the number of impacts increases, the delamination area in the composite laminate rises (see Fig. 7 which is plotted for initial impactor's energy of 6 J). The propagation of delamination shows two regions: an initial rapid growth in the beginning and a far slower growth after around 6 IPL (Fig. 7). This can be explained by the fact that, in the first region, a great part of impact energy is absorbed by delamination which is relatively proportional to the received energy from the impactor(s) [44]. In the second region, each impact results in less incremental delamination. In this region, after a certain number of impacts, the phenomena of delamination saturation happens [33]. This part of the damage curve is relatively horizontal (i.e. a plateau is reached) illustrating the slowdown of delamination process caused by damage [45].

3.3. Effect of impact spacing

To determine whether or not the distance between hail impactors affects the delamination area and link-up region, two impact locations with varying distances between them were examined (see Fig. 8). It is worth mentioning that the hail impactors had the same impact energy in each location, and the delamination area was measured after 5 impacts per location (5IPL). The delamination areas form due to the stress wave propagating through the thickness towards the back side of the plate and then reflecting from the rear face during the impact process. The area closest to the rear face is the first region subjected to tensile stress, which leads to interlayer delamination damage tendency to occur in the rearest interlayer [46]. With increasing the number of impacts or the incoming impactor's energy level, the interlayer delamination damage propagates from the rear face to the front surface [47].

Fig. 9 illustrates the delamination area versus distance between hail impactors for four energy levels (6, 8, 10, and 13 J). For all impact energies, there exists a link-up delamination area for very small spacing. It can be observed that by increasing the distance between the hail
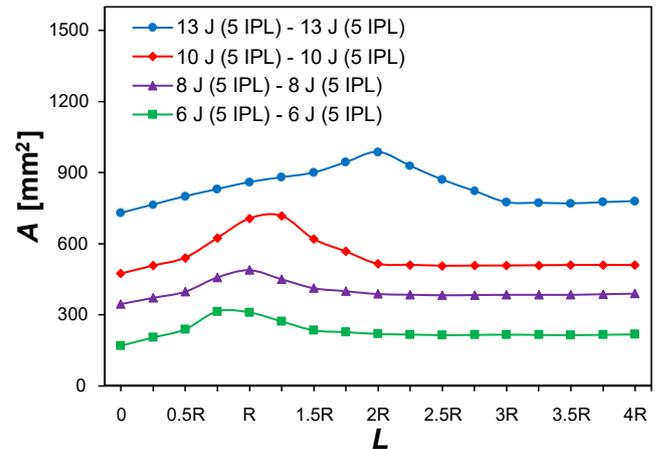
Fig. 9. Comparison of delamination areas under different impact energies (two-point impact and 5 impacts per location).

(a)   (b)   (c)

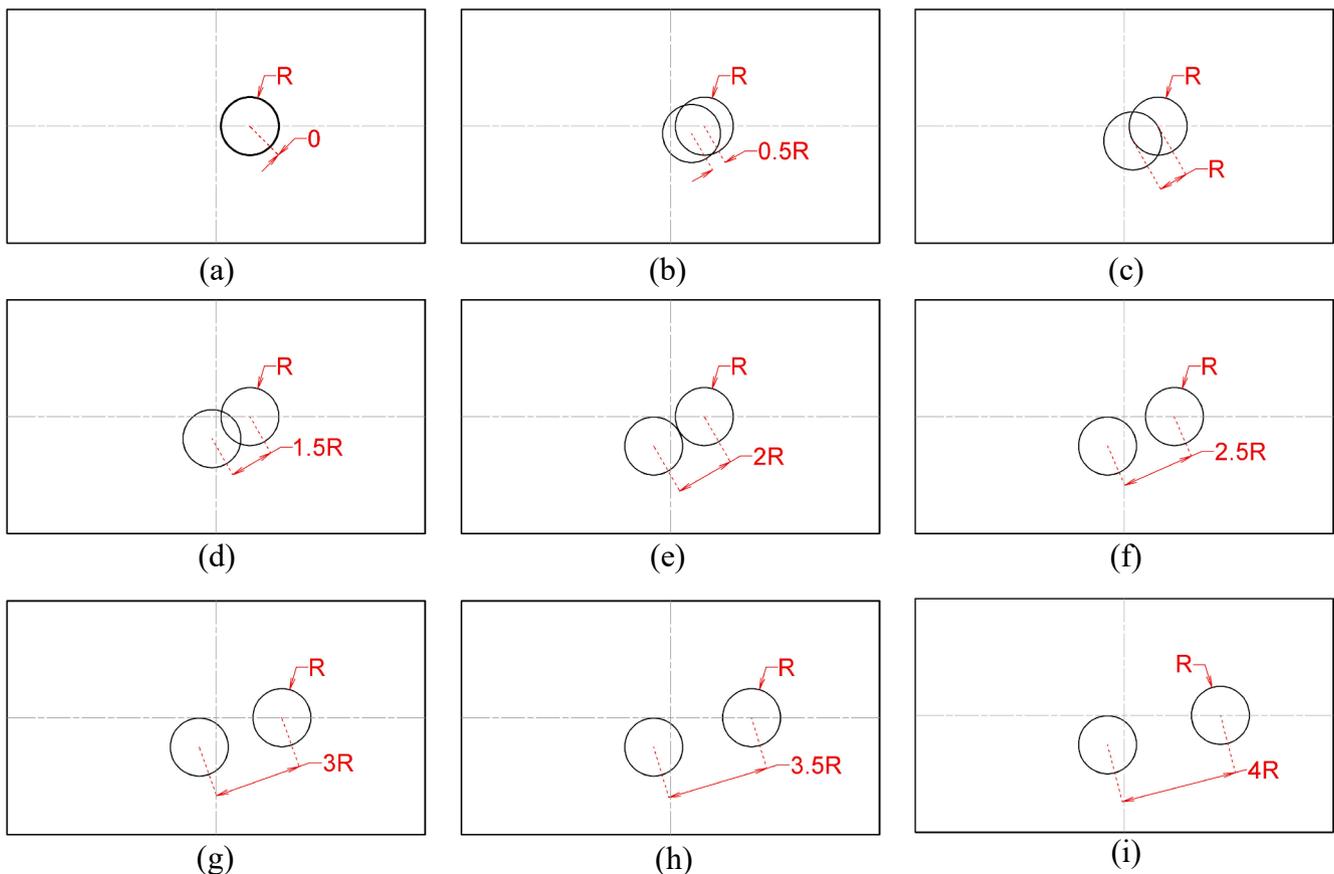(d)   (e)   (f)

(g)   (h)   (i)

Fig. 8. Different spacings studied for link-up.

impactors, the delamination zone grows until the link-up disappears (Fig. 9). After the disappearance of the link-up region, the delamination area shows a drop, and then the curve tends to flatten. This is schematically illustrated in Fig. 10. As a typical result, there appears to be a period of initial growth in delamination area, reaching its highest point at the link-up threshold. It is then followed by a decline until a plateau region is reached where the delamination area continues to remain constant. This phenomenon can be explained by the fact that the overlapped delamination region caused by double-position impacts gradually separates as the impact distance increases from zero to a threshold value [48]. After the threshold point (the link-up threshold), as the distance between the impact points increases, the extent of damage decreases radically [47], as the direct interaction between two impact locations disappears.

It can be observed that the area delaminated by two consecutive hailstone impacts at the same location (Point A_1 in Fig. 10) is smaller than that delaminated by two hailstone impacts at two (far-away) independent locations (Region A_3 in Fig. 10). If we denote the delaminated area in each impact location by A_i, the results show that $A_1 < 2A_i$ and $2A_i < A_2$. This is in accordance with what has been observed in several other works [33]. The relationship $A_1 < 2A_i$ can be explained by the fact that when a location becomes delaminated due to a first set of impacts, the extent of extra delamination due to the second set of impacts reduces, as the laminate has already been delaminated to a high extent after the first set of impacts. Moreover, $2A_i < A_2$ can be explained by the additional damaging effect of the link-up phenomenon as compared to the case of two independent locations being impacted. This can be explained by the fact that when the laminate is impacted at two independent locations, there is no direct interaction between delaminated regions and the delamination area (A_3) is almost twice the delamination area of each independent location ($A_3 \approx 2A_i$). In addition, due to the effect of link-up on the area of delamination, A_2 (see Fig. 10) is much greater than the delamination area in other spacings.

It is obvious that the area of delamination and the link-up region should enlarge with increasing the impact energy. The maximum spacing for which link-up areas can be observed is $0.75R$ for the impact energies of 6 J, R for 8 J, $1.25R$ for 10 J, and $2R$ for the impact energies of 13 J. In addition, it could be observed that at the link-up threshold spacing, the delamination area under 13 J impact energy is 21% higher than that under 10 J energy, which is in accordance with the fact that the increasing impact energy expands the area of delamination.
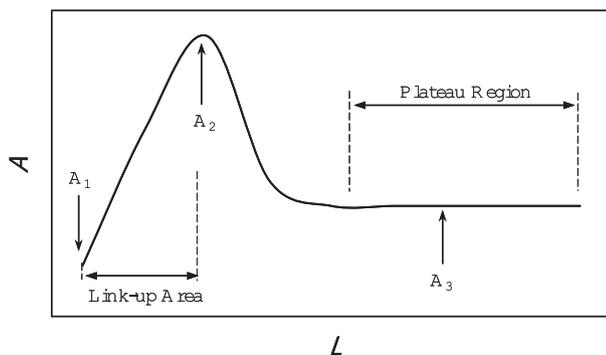
3.4. Effect of impact energy

To study the effect of having non-identical energy levels at each impact location, three impact scenarios were investigated. The impactor energy at locations one and two are set to 13 J-10 J, 14 J-6 J, and 10 J-6 J. As it can be seen in Fig. 11, the overall trend of the $A-L$ curves for impactor with non-identical energy is very similar to the trend of impactors with identical energy levels (which are represented by grey dashed curves in Fig. 11). Increasing the impact energy of the second point from 6 J to 10 J, while maintaining the impact energy of the first point around 13 J, increased the threshold link-up area spacing from $1R$ to $1.5R$. The other point of interest is studying the effect of asymmetry in the energy level of two impactors, while the total energy received by the laminate is kept constant. Two parametric studies with total impact energies of 20 J and 16 J have been considered for this purpose and are discussed in the following paragraphs.

As for the first case, the difference in the link-up threshold between the two-point sequential impacts of 10 J (5IPL)-10 J (5IPL), 14 J (5IPL)-6 J (5IPL), and 16 J (5IPL)-4 J (5IPL) all receiving the same total impact energy of 20 J (5IPL) is investigated, see Fig. 12. The figure shows that the link-up threshold spacing in 10 J (5IPL)-10 J (5IPL) is 1.25R and in other two cases is identical and equal to 1R, whereas they show some differences in the delamination area. By changing the impact energies from 10 J (5IPL)-10 J (5IPL) to 16 J (5IPL)-4 J (5IPL), i.e. 60% change in the energy level at each impact location, the delamination area at link-up threshold decreases for 55%. However, changing the impact energies from 14 J (5IPL)-6 J (5IPL) to 16 J (5IPL)-4 J (5IPL), i.e. a maximum of 34% change in the energy level at each impact location, the delamination area at link-up threshold decreases for 7% only. This can be explained as follows. As the first impactor's energy is decreased by a particular amount (e.g. 4 J), the local delamination area decreases, as expected. Keeping in mind that the total energy level caused by two impactors must be kept constant, the energy of the second impactor has to be increased by the same amount (i.e. 4 J). However, the increase in the local delamination area at the second point does not compensate for decrease in the delamination area in the first impact location due to delamination saturation phenomenon in the second point, and hence the total delamination area decreases.

As for the second case, the delamination observations for the two-point sequential impacts of 8 J (5IPL)-8 J (5IPL), 10 J (5IPL)-6 J (5IPL), and 12 J (5IPL)-4 J (5IPL) in Fig. 13 all receiving the same total impact energy of 16 J (5IPL) are interesting. The link-up threshold spacing of the case of 10 J (5IPL)-6 J (5IPL) is similar to that of 12 J
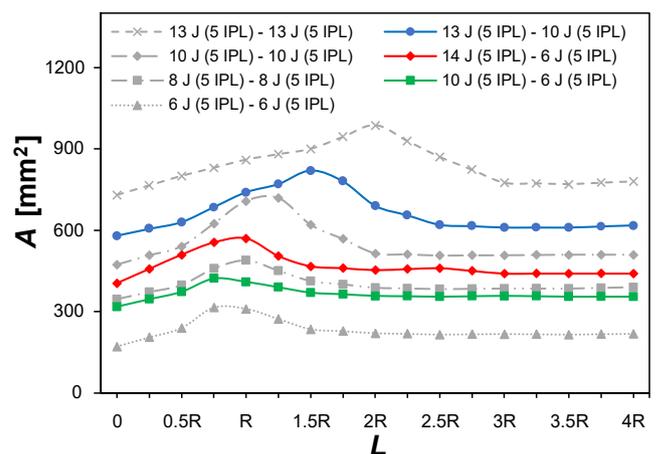

Fig. 10. The typical trend of variation of delamination area with respect to the spacing between impactors. A_1 indicates the delamination area caused by the impact of two consecutive hailstones on a single location. A_2 represents the threshold delamination area, occurring when two consecutive hailstones impact two distinct locations with the highest potential to influence each other (i.e. the highest link-up area). A_3 denotes the delamination area resulting from the impact of two consecutive hailstones on two independent locations, where there is no direct interaction between them, and hence no link-up delamination occurs.

Fig. 11. Comparison of delamination areas under different impact energies. In each total impact level, the impactors have both identical and non-identical energy levels. It can be observed that the scenarios in which the two impactors have symmetrical energy levels (grey dashed curves) show a similar trend to scenarios in which the two impactors have non-symmetrical energy levels.
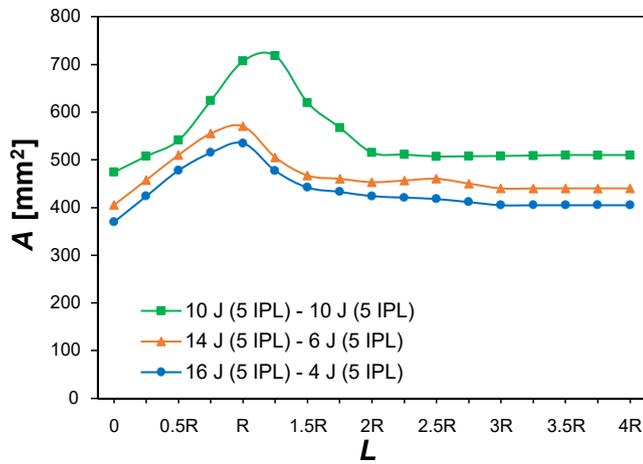
Fig. 12. Comparison of delamination area for symmetrical and non-symmetrical impactor energy distribution for the total impact energy of 20 J.
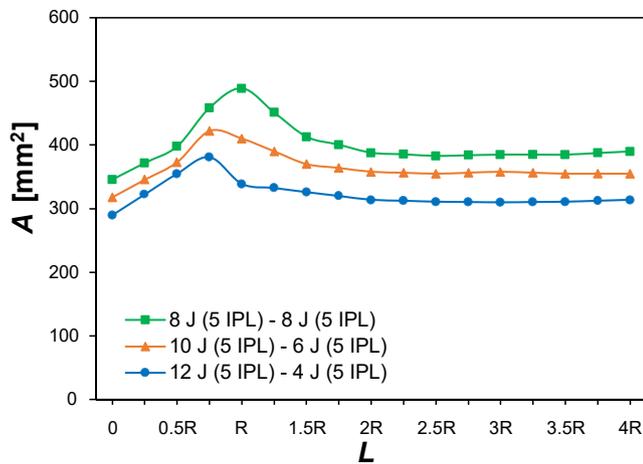

Fig. 13. Comparison of delamination area for symmetrical and non-symmetrical impactor energy distribution for the total impact energy of 16 J.

(5IPL)-4 J (5IPL), while the delamination area in the former is 8% higher. On the other hand, decreasing the impact energy of the second point from 8 J to 6 J (when the total impact energy is constant) reduces the threshold link-up area spacing from $1R$ to $0.75R$. Generally, it can be concluded that for the same total impact levels, scenarios having impactors with non-identical energy levels have lower delamination area as compared to the case of impactors with the same energy levels. Moreover, increasing the asymmetry in the energy levels of two impactors tends to decrease the link-up spacing threshold. It is noteworthy that, provided that the panel has not been previously damaged or impacted, although low-energy impactors (e.g. 4 J) are not likely to cause any critical damage in the laminate, when combined with another impactor, they can increase the sustained damage substantially. The relatively high damage sustained by the 4 J impactor when combined with 16 J impactor and 12 J impactor are visible in Fig. 12 and Fig. 13, respectively.

Fig. 14 demonstrates the effect of impactor's initial energy on the force–time diagrams for a single impact location. As it can be seen, increasing the impactor's initial energy leads to higher maximum force (F_{max}) and lower contact duration, similar to what has been observed in other works [49,50]. For example, by increasing the impactor's energy from 10 J to 13 J (30% increase), the peak force increased by 22% and the contact duration decreased by 4%. Increasing the impactor's initial energy also led to an earlier relative peak time (as compared to total
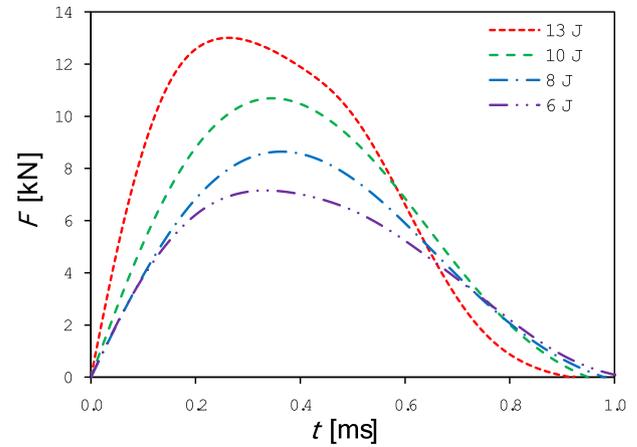

Fig. 14. Effect of impactor's initial energy on the force–time diagram.

impact duration in each case) and, as a result, a more left-skewed bell shape for the force–time curve. Similarly, Çoban et al. [51] reported that by increasing the impactor's energy not only the peak force increases, but the symmetry of the F-t curves disappears.

3.5. Effect of number of impacts

The effect of changing the number of impacts per location (IPL) on the delamination area and link-up region under hail impact was also studied. Here, multiple impacts at two points with the same energy levels but different numbers of impact per location are considered. One point was impacted 5 times while the number of impacts at the other point was varied. As for the delamination curves in Fig. 15, Fig. 16, and Fig. 17, a growing delamination area is observed with the increase in the number of impacts. For the case of impact energy of 6 J, while increasing the number of impacts for the second location increased the delamination area, it did not succeed to increase the threshold link-up area spacing (Fig. 15). However, for the case 13 J impact energy (Fig. 17), increasing the number of IPL for the second point from 1 to 3 and then 5 increased the threshold link-up area spacing from $0.75R$ to $1.5R$ and $2R$. This can be explained by the fact that for the case of low energy level and 5IPL-5IPL (blue curve in Fig. 15), a very low link-up threshold value (i.e. $L_{th} = 0.75R$) is observed making it difficult to reach smaller link-up threshold values for smaller number of IPL.
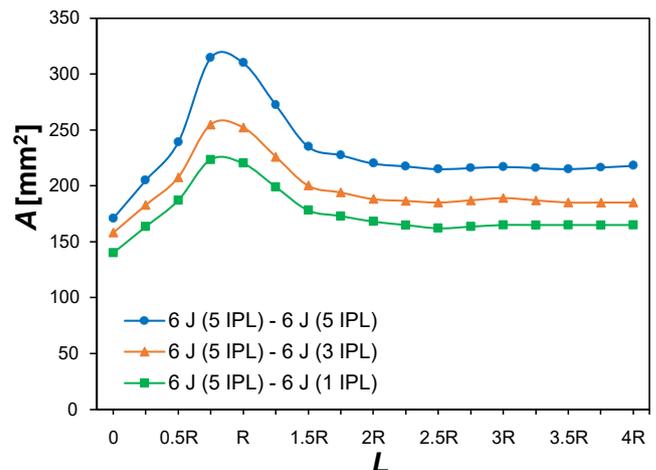

Fig. 15. Comparison of delamination areas under different impacts per location (6 J).
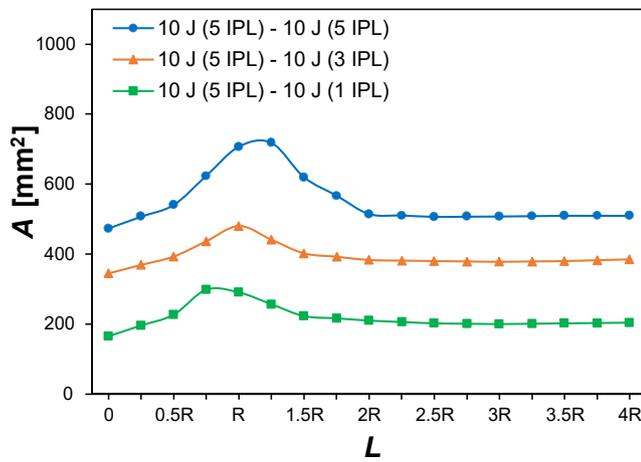
Fig. 16. Comparison of delamination areas under different impacts per location (10 J).
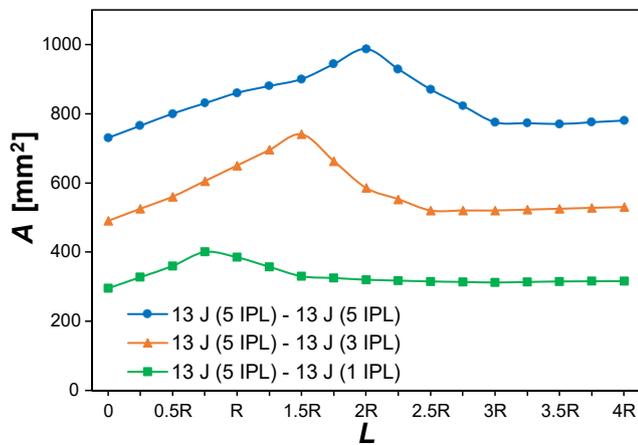

Fig. 17. Comparison of delamination areas under different impacts per location (13 J).

3.6. Effect of number of impact locations

Studying the number of impact locations gives a good insight for assessing the capability of the composite plate to resist hailstorms with different severities. The area of delamination damage under the same impact energy (6 J) but with different impact schemes is compared in Fig. 18 and Fig. 19. In addition to the effect of number of impact locations, the influence of impact spacing on the delamination area was also studied. Increasing the number of impact locations led to proportional increase in delamination area for both spacings of R and $2R$ (Fig. 20). For instance, changing the number of impact locations from 3 to 4 resulted in the 33% increase in the delamination area for the spacing of R (Fig. 18). As shown in Fig. 9 for two impacts each having an energy level of 6 J, delaminations linked up when the distance between the impact locations was equal to R or less. A similar phenomenon was observed for higher impact locations (i.e. for 3–6 impact locations), see Fig. 18. The link-up phenomenon in the spacing of R had a very significant influence on the increase in the measured delamination area in comparison to the cases where the spacing was $2R$, leading to more severe damage in this case (see Fig. 20). For instance, for the case of 3 impact locations, the delamination area was 62% higher for $L = R$ as compared $L = 2R$, which can lead to a remarkable reduction in damage resistance. As it can be seen in Fig. 9 and Fig. 19, for the impactors with initial energy of 6 J and for the impact spacing of $L = 2R$, there is no direct interaction between delaminated regions (and as a result, there is no link-up) for all

number of impact locations (from 2 to 6 separate impacts). It is worth noting that for the case of 5 and 6 impact locations in $L = 2R$, where the impactor impacts the regions near the clamping edges, a boundary effect starts appearing which can be observed visually as an increase in the delamination area in both regions (see Fig. 19c and Fig. 19d). Later on, and with more number of impacts, this boundary effect might lead to abrupt and exponential advances in damage extent.

Fig. 21a compares the force–time contact diagrams of the composite laminate subjected to different number of impactors (each impactor having the same initial energy of 6 J). A higher number of impact locations results in a higher maximum contact force and stiffness. With increasing the number of impact locations, the maximum recorded contact force and slope of curves increased. The peak force F_{max} for 1, 2, 3, 4, 5, and 6 impact locations was 0.72 kN, 1.39 kN, 2.20 kN, 3.16 kN, 3.74 kN, and 4.33 kN, respectively. The maximum contact force had a relatively linear correlation with the number of impact locations (see Fig. 21b). All the force–time curves had relatively symmetrical shapes with their force values reaching their peak at the mid-time of the impact.

4. Discussions

4.1. Fatigue response

The results of our study show that after a certain number of impacts, the delamination growth starts slowing down (see Fig. 7 which shows the decrease in the delamination area growth rate after the 8th impact). We increased the number of impacts to 20 impacts, which showed that the delamination area growth rate decreases even further. Similarly, Liao et al. [48] and Azouaoui et al. [44] observed that at low energy levels, delamination propagates slowly even with the increase in the number of impacts. This trend will not likely continue if the number of impacts is increased to very large numbers. In the case of very large number of impacts, other damaging mechanisms such as low-cycle fatigue or high-cycle fatigue may come into play. This would lead to an exponential increase in the delamination area after a threshold number of impacts [51–53]. Overall, three regions can be identified in the impact-indeced fatigue scenario: first impacts create obvious damage in matrix leading to cracking, delaminations and/or fibre fracture, followed by a plateau in which damage increments marginally under successive impacts. Finally, in the third region, the damage develops rapidly and fibres fracture towards final failure [33]. The fatigue-induced catastrophic damages are caused by highly repeated small hailstone impacts which usually do not generate observable damages or penetrations. The failure behavior of composite panels in low-cycle and high-cycle fatigue regimes is therefore an interesting field of study for future works.

4.2. Possible variations in hail size and distribution

As stated earlier, the literature generally considers a diameter of 0.5 cm to be the boundary between graupel and hail. Nearly 40% of the reports containing gathered information on the largest hail size reported maximum hailstones in the range of 2–2.9 cm. Despite the fact that<10% of these reports had hails greater than 5 cm, hailstones with diameters in the range of 15 cm have been reported recently [5]. Additionally, Giaiotti et al. [54] demonstrated that, in 20% of the times, hailstone overlap occurs, although the overlap decreases with increase in the hailstone size. Thus, hail impact models can be changed from numerous impacts in various areas to single impacts in multiple locations, along with the above description of damage growth upon repeated impacts. This will greatly reduce the complexity of hail simulations and experiments while basing them on more reliable observations [38].

4.3. Effect of distribution of energy

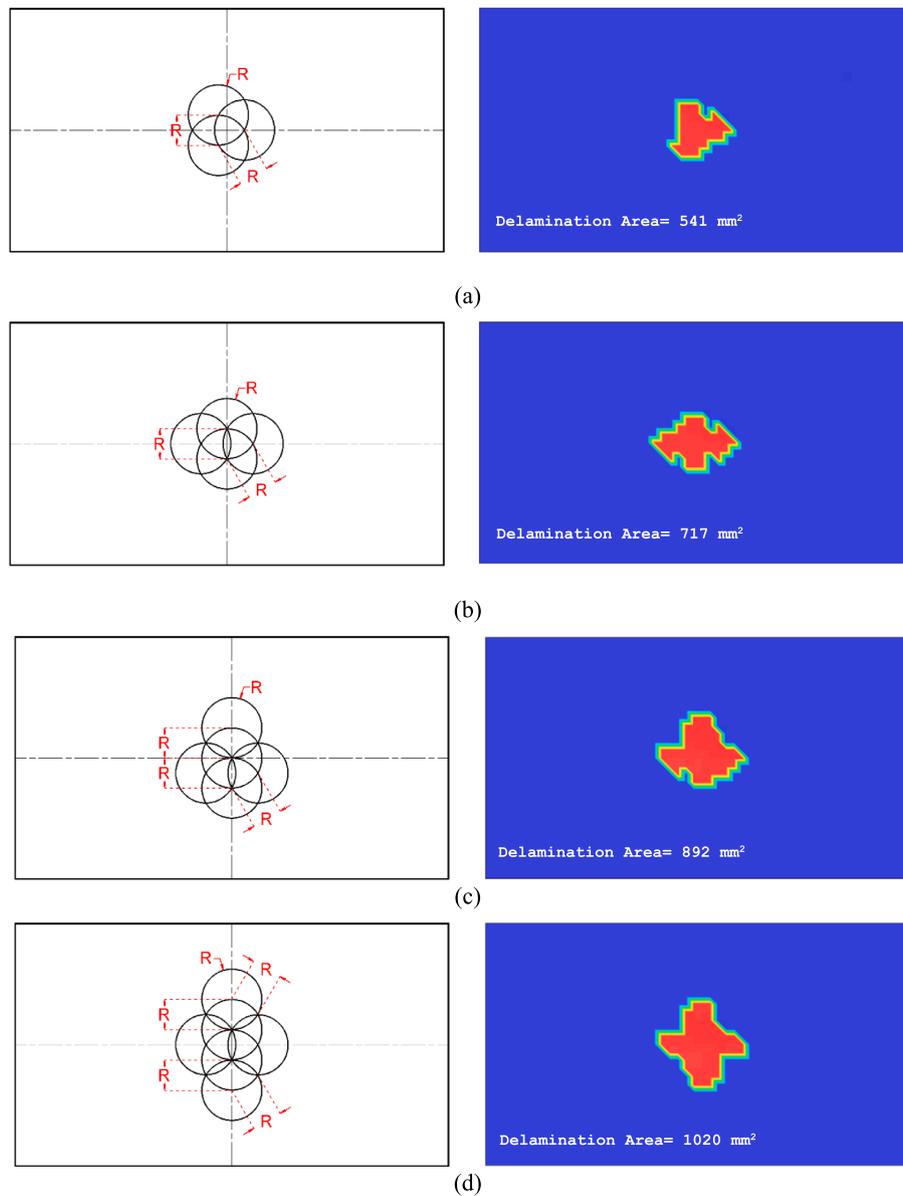In this study, two impact locations underwent symmetrical and non-

Fig. 18. Impact locations arrangement (left) and delamination areas (right) for the spacing of **R**. (a) 3, (b) 4, (c) 5, and (d) 6 impact locations.

symmetrical variations in terms of the quantity of impacts per location and the impactor energy. The results showed that as the impact energy increased the threshold spacing for link-up along with the delamination area increased. For the case of impact at two locations while keeping the total energy level constant, two impactors with identical energy level lead to higher delamination areas as compared to impactors with non-identical energy levels. Additionally, the link-up spacing threshold tends to decline as the energy levels of two impactors become more non-symmetrical. It is noteworthy that although low-energy impactors (in this work, 4 J) are not expected to produce any critical damage in the laminate assuming the panel has not already been damaged or affected, when paired with another impactor, they can significantly increase the sustained damage.

4.4. SPH vs other numerical approaches

In high velocities, the hail stones have a fluid-like behavior. That is why, as mentioned earlier, several numerical approaches such as Lagrangian [55–58], ALE [6], SPH [59], and SHI approaches have been used in different studies for modelling the ice impact. The Lagrangian method is a well-known approach for modelling solid objects and in circumstances where deformation extents are limited. That is why although the Lagrangian method requires much less modelling effort, the large deformations and extreme distortions the elements experience during the hail impact duration creates unacceptable inaccuracies in the results. Extreme element distortions not only create inaccuracies in the results, they also decrease the minimum element size in the FE model which increases the computational time exponentially usually leading to early numerical errors.

To overcome the described large element distortions, the ALE method, which uses the advantages of both the Eulerian and Lagrangian methods, can be used. In the Eulerian method, the material can freely move inside a mesh fixed in space. In the ALE method, depending on the flow of the material, the mesh location is adjusted arbitrarily in the space leading to lower computational time required if the material moves over a relatively large domain. That is why, unlike the Lagrangian method, in the ALE method, large distortions are not of concern. Nonetheless, this approach usually requires a good knowledge of many involving numerical parameters, especially for imposing an accurate coupling between the fluid in the ALE domain and the target in the
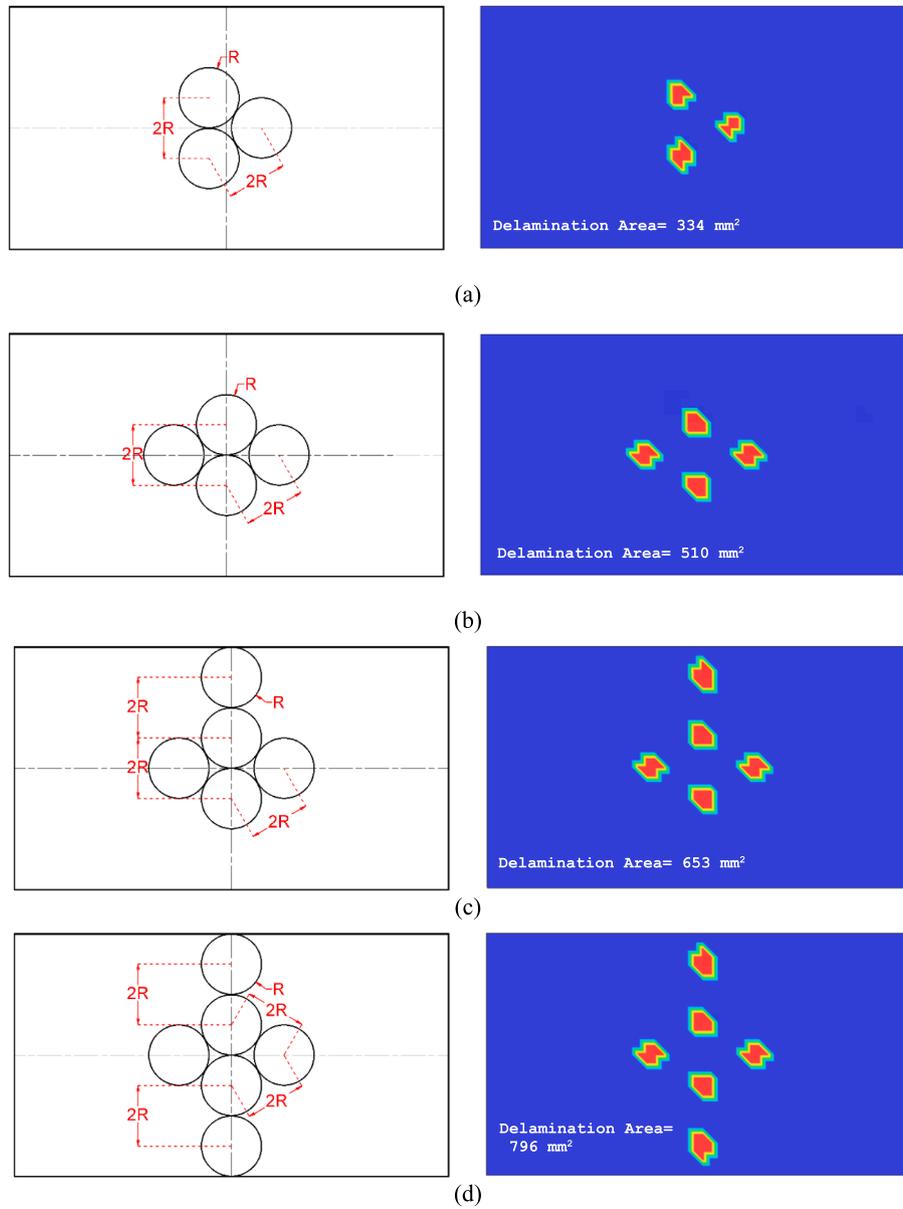
Fig. 19. Impact locations arrangement (left) and delamination areas (right) for the spacing of 2*R*. (a) 3, (b) 4, (c) 5, and (d) 6 impact locations.
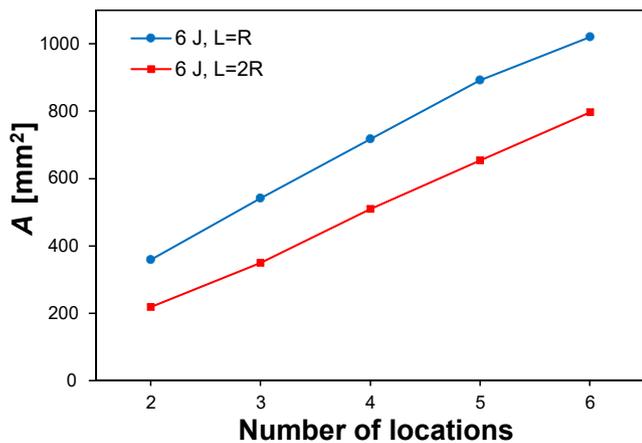

Fig. 20. Variation of delamination area with respect to the number of impact locations (for impactor energy of 6 J). The fitting curves are $A_n = 167.5n + 203.1$ and $A_n = 145.5n + 69.3$ for $L = R$ and $L = 2R$.

Lagrangian domain, see [3] for further information.

The SPH method on the other hand is a mesh-less approach in which a mass value is assigned to discrete particles each representing small fluid volumes. Each particle interacts with its neighboring particles through interpolating functions (known as kernel functions) [60]. Our initial investigations as well as other research works have shown the higher effectiveness of the SPH method from both the computational time and accuracy points of view. In the case of hail impacts with lower velocities, Lagrangian method can become more efficient than the SPH method since the hail might not undergo fluid-like behavior.

4.5. Composite design aspects

The results showed that as the distance between the impact location and the plate boundaries decreases, the induced damage area increases. One could argue that adding supporting repair patches in the boundary of the panels can help reduce the delamination area. Other considerations, however, also need to be taken into account. Transition from thin to thick plates can lead to stress concentration at the transition points/ edges. Moreover, stiffer (thicker) target plates can reduce the resulting
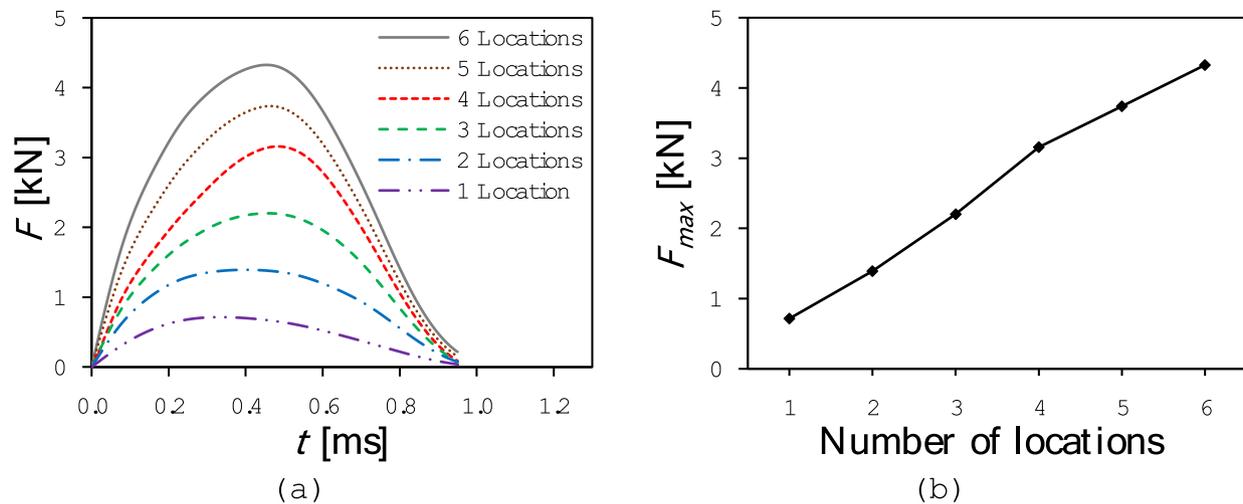
Fig. 21. (a) Effect of number of impact locations on the force vs time curves. (b) Correlation of peak-force with number of impact locations (for impactors each having the initial energy of 6 J).

displacement and hence increase the peak force which could localize the failure region further, and hence increase the damage extent. Studying the effect of having thicker plates, plates with multiple thickness values, and effect of different composite material properties is suggested for future studies where design for improvement against hail impact can be defined as the main goal.

4.6. Climate change considerations

Climate change modifies the environment in which the hail stones are formed and grown. Three important characteristics of the environment will change as a response to climate effects: vertical wind shear, melting level height, and low-level moisture and as a result convective instabilities [61]. Convective storms that generate the hailstorms are particularly of much higher importance among the three noted effects. Due to global warming, the water vapor content in the atmosphere is increasing (7% per °C) which in turn would increase the potential energy that can be released through convective instability and leading to formation of larger hailstones. Even 1 °C increase in the temperature could lead to thunderstorm initiation [62]. Increase in the temperature of near-surface temperature due to solar radiation and advection of the heated air can also be influential in increased thermal instabilities and, as a result, the formation of hailstorms [39]. Studying the past trends and developing of models for future trends has shown the increase the hailstorm frequency, intensity, and size in Europe [63,64], Australia [65], and dry and cool regions of North America [66]. The kinetic energy of a hail stone increases with the third power of its diameter. In the near future, this can drastically increase the imposed damage on the composite panels in the form of wear, delamination, and even penetration.

5. Conclusions

In this study, the response of a 16-ply carbon fibre prepeg composite plate to ice projectiles at one or multiple impact locations was studied. Special attention was paid to delamination area and more importantly the link-up delamination area. Link-up of delamination is defined as the phenomenon of joining separate delamination regions as a result of different impactors. The number of impacts per location, the impactor energy, and the spacing between impact locations was varied symmetrically and non-symmetrically for two impact locations. Based on the results for delamination area, the following conclusions can be made:

- As a general observation, as the spacing L between *two* impact location increases from 0 to 4R, the delamination area first shows an increase up to a peak point (usually at $R < L < 2R$) after which it shows a large drop leading to flattening in the delamination area curve. The large drop is related to disappearance of link-up phenomenon after a certain spacing.
- If IPL in one location is set to five, and the number of IPL for the other point is increased from 1 to 5, the delamination area almost doubles.
- Increasing the number of impact locations increases the delamination area linearly.

Regarding the link-up phenomenon, the following conclusions can be made:

- As the impactor energy increases, the threshold spacing for link-up disappearance increases.
- At the same total energy level, as compared to the case with impactors having the same energy level, having impactors with non-identical energy levels leads to a lower delamination area and lower threshold link-up area spacing.
- Regardless of the number of impact locations, if the impact spacing is smaller than a threshold value (e.g. $L \leq R$ for impactor energy of 6 J), the link-up phenomenon appears which leads to significant enlargement in the delamination area leading to more severe damage. In impact spacings larger than that threshold value, increasing the number of impact locations does not affect the appearance of the link-up phenomenon.

CRediT authorship contribution statement

Mojtaba Sadighi: Conceptualization, Methodology, Validation, Formal analysis, Writing – original draft, Writing – review & editing, Supervision. **René Alderliesten:** Conceptualization, Validation, Formal analysis, Writing – review & editing, Supervision. **Azadeh Fathi:** Methodology, Software, Formal analysis, Writing – original draft, Writing – review & editing, Visualization. **Babak Soltannia:** Methodology, Software, Writing – review & editing, Supervision. **Reza Hedayati:** Methodology, Software, Validation, Formal analysis, Writing – original draft, Writing – review & editing, Supervision.

Declaration of Competing Interest

The authors declare that they have no known competing financial interests or personal relationships that could have appeared to influence

the work reported in this paper.

Data availability

Data will be made available on request.

References

[1] Olsson R, Juntikka R, Asp LE. High velocity hail impact on composite laminates–modelling and testing. In: Dynamic failure of composite and sandwich structures. Springer; 2013. p. 393–426.

[2] Hedayati R, Sadighi M. Effect of using an inner plate between two faces of a sandwich structure in resistance to bird-strike impact. J Aerosp Eng 2016;29(1): 04015020.

[3] Hedayati, R. and M. Sadighi, Bird strike: an experimental, theoretical and numerical investigation. 2015: Woodhead Publishing.

[4] Hedayati R, Ziaei-Rad S. Foam-core effect on the integrity of tailplane leading edge during bird-strike event. J Aircr 2011;48(6):2080–9.

[5] Ganesh Ram, S., Can Hail Impacts Trigger Delaminations?: A qualitative study to evaluate the consequences of hail ice impact on composite structures. 2021.

[6] Anghileri M, et al. A survey of numerical models for hail impact analysis using explicit finite element codes. Int J Impact Eng 2005;31(8):929–44.

[7] Mahinfalah M, Skordahl RA. The effects of hail damage on the fatigue strength of a graphite/epoxy composite laminate. Compos Struct 1998;42(2):101–6.

[8] Dieling C, et al. Hail impact testing: velocity effects of distance to target specimen. J Wind Eng Ind Aerodyn 2021;211:104554.

[9] Walton, J. Where are all the unused planes right now? 2020 2022.

[10] Dessens J, Berthet C, Sanchez J. Change in hailstone size distributions with an increase in the melting level height. Atmos Res 2015;158:245–53.

[11] Combescure A, Chuzel-Marmot Y, Fabis J. Experimental study of high-velocity impact and fracture of ice. Int J Solids Struct 2011;48(20):2779–90.

[12] Cai W, Zhu L, Qian X. Dynamic responses of steel plates under repeated ice impacts. Int J Impact Eng 2022;162:104129.

[13] Cai W, et al. Numerical simulations for plates under ice impact based on a concrete constitutive ice model. Int J Impact Eng 2020;143:103594.

[14] Chen S, et al. Experiments on an ice ball impacting onto a rigid target. Int J Impact Eng 2022:104281.

[15] Kim H, Kedward KT. Modeling hail ice impacts and predicting impact damage initiation in composite structures. AIAA J 2000;38(7):1278–88.

[16] Appleby-Thomas GJ, Hazell PJ, Dahini G. On the response of two commercially-important CFRP structures to multiple ice impacts. Compos Struct 2011;93(10): 2619–27.

[17] Kim H, Welch DA, Kedward KT. Experimental investigation of high velocity ice impacts on woven carbon/epoxy composite panels. Compos A Appl Sci Manuf 2003;34(1):25–41.

[18] Park H, Kim H. Damage resistance of single lap adhesive composite joints by transverse ice impact. Int J Impact Eng 2010;37(2):177–84.

[19] Rhymer J, Kim H, Roach D. The damage resistance of quasi-isotropic carbon/epoxy composite tape laminates impacted by high velocity ice. Compos A Appl Sci Manuf 2012;43(7):1134–44.

[20] Dolati S, Fereidoon A, Sabet AR. Experimental investigation into glass fiber/epoxy composite laminates subjected to single and repeated high-velocity impacts of ice. Iran Polym J 2014;23(6):477–86.

[21] Tang Z, et al. Numerical and experimental investigation on hail impact on composite panels. Int J Impact Eng 2017;105:102–8.

[22] Kim H, Keune JN. Compressive strength of ice at impact strain rates. J Mater Sci 2007;42(8):2802–6.

[23] Tippmann JD, Kim H, Rhymer JD. Experimentally validated strain rate dependent material model for spherical ice impact simulation. Int J Impact Eng 2013;57: 43–54.

[24] Carney KS, et al. A phenomenological high strain rate model with failure for ice. Int J Solids Struct 2006;43(25–26):7820–39.

[25] Chuzel Y, et al. Development of hail material model for high speed impacts on aircraft engine. In: 11th international LS-Dyna users conference; 2010.

[26] Fathi A, et al. Experimental investigation of quasi-static behavior of composite and fiber metal laminate panels modified by graphene nanoplatelets. J Reinf Plast Compos 2021;40(13–14):518–32.

[27] Wu X, et al. Dynamic responses and energy absorption of sandwich panel with aluminium honeycomb core under ice wedge impact. Int J Impact Eng 2022;162: 104137.

[28] Roudbarian N, et al. Enhancing shape memory properties of multi-layered and multi-material polymer composites in 4D printing. Smart Mater Struct 2021;30 (10):105006.

[29] Torkestani A, Sadighi M, Hedayati R. Effect of material type, stacking sequence and impact location on the pedestrian head injury in collisions. Thin-Walled Struct 2015;97:130–9.

[30] Zhang P, et al. Phase field modeling of fracture in fiber reinforced composite laminate. Int J Mech Sci 2019;161:105008.

[31] Allegri, G., Failure in composites: Filling the knowledge gaps, in ACCIS 2018 Conference. 2018.

[32] Rezasefat M, et al. Numerical study on the dynamic progressive failure due to low-velocity repeated impacts in thin CFRP laminated composite plates. Thin-Walled Struct 2021;167.

[33] Sadighi M, Alderliesten R. Impact fatigue, multiple and repeated low-velocity impacts on FRP composites: a review. Compos Struct 2022;297.

[34] Juntikka R, Olsson R. Experimental and modelling study of hail impact on composite plates. In: Proceedings of The 17th International Conference of Composite Materials; 2009. p. 27–31.

[35] Monaghan JJ. Smoothed particle hydrodynamics. Ann Rev Astron Astrophys 1992; 30:543–74.

[36] Gingold RA, Monaghan JJ. Smoothed particle hydrodynamics: theory and application to non-spherical stars. MNRAS 1977;181(3):375–89.

[37] ASTM, D7136/D7136M − 15 Standard Test Method for Measuring the Damage Resistance of a Fiber-Reinforced Polymer Matrix Composite to a Drop-Weight Impact Event. 2015.

[38] Verstraeten, D., Hail Impact on Composite Aircraft: Investigation of low-velocity impacts in multiple impact locations and the effect on its fatigue life. 2019.

[39] Punge HJ, Kunz M. Hail observations and hailstorm characteristics in Europe: a review. Atmos Res 2016;176:159–84.

[40] Púčik T, et al. Large hail incidence and its economic and societal impacts across Europe. Mon Weather Rev 2019;147(11):3901–16.

[41] Saul M, Lunford L. *Damage from grounds nearly 100 D/FW planes passengers scramble as scores of flights cancelled* in *dallas morning*. News 1995.

[42] Feraboli P, et al. LS-DYNA MAT54 modeling of the axial crushing of a composite tape sinusoidal specimen. Compos Part a-Appl Sci Manuf 2011;42(11):1809–25.

[43] Sy BL, Fawaz Z, Bougherara H. Numerical simulation correlating the low velocity impact behaviour of flax/epoxy laminates. Compos Part a-Appl Sci Manuf 2019; 126.

[44] Azouaoui K, et al. Damage characterisation of glass/polyester composite plates subjected to low-energy impact fatigue. J Sound Vib 2007;308(3–5):504–13.

[45] Azouaoui K, et al. Modelling of damage and failure of glass/epoxy composite plates subject to impact fatigue. Int J Fatigue 2001;23(10):877–85.

[46] Zhu X, et al. Damage mechanism of composite laminates under multiple ice impacts at high velocity. Int J Impact Eng 2022:104296.

[47] Zhu X, et al. Damage mechanism of composite laminates under multiple ice impacts at high velocity. Int J Impact Eng 2022;168.

[48] Liao B, et al. Effect of double impact positions on the low velocity impact behaviors and damage interference mechanism for composite laminates. Compos. Part A Appl. Sci. Manuf 2020;136:105964.

[49] Fathi A, Liaghat G, Sabouri H. An experimental investigation on the effect of incorporating graphene nanoplatelets on the low-velocity impact behavior of fiber metal laminates. Thin-Walled Struct 2021;167.

[50] Zarei H, et al. Low velocity impact damage assessment of GLARE fiber-metal laminates interleaved by Nylon 6,6 nanofiber mats. Compos Struct 2017;167: 123–31.

[51] Çoban O, et al. Fracture morphology and deformation characteristics of repeatedly impacted thermoplastic matrix composites. Mater Des 2009;30(3):628–34.

[52] Wyrick D, Adams D. Damage sustained by a carbon/epoxy composite material subjected to repeated impact. Composites 1988;19(1):19–27.

[53] Azouaoui K, Azari Z, Pluvinage G. Evaluation of impact fatigue damage in glass/ epoxy composite laminate. Int J Fatigue 2010;32(2):443–52.

[54] Palencia C, et al. Dent overlap in hailpads: error estimation and measurement correction. J Appl Meteorol Climatol 2011;50(5):1073–87.

[55] Cui Q, Yang J. Evaluation of numerical simulation methods and ice material models for intermediate-velocity hail impact simulation. Eng Struct 2021;244: 112831.

[56] Hedayati R, Jahanbakhshi M. Finite element analysis of an aluminum airplane stabilizer against birdstrike. J Braz Soc Mech Sci Eng 2016;38:317–26.

[57] Liu C, et al. Impact of saddle membrane structure by hail with combined particle sizes: numerical simulation and experimental investigation. Eng Struct 2022;264: 114477.

[58] Saini D, Shafei B. Prediction of extent of damage to metal roof panels under hail impact. Eng Struct 2019;187:362–71.

[59] Mintu, S. and D. Molyneux. Simulation of ice-structure interactions using a coupled SPH-DEM method. in OTC Arctic Technology Conference. 2018. OnePetro.

[60] Hedayati R, Ziaei-Rad S. New bird model for simulation of bird strike on various layups used in transparent components of rotorcrafts. J Aerosp Eng 2014;27(1): 76–85.

[61] Raupach TH, et al. The effects of climate change on hailstorms. Nat Rev Earth & Environ 2021;2(3):213–26.

[62] Warren, S., et al. Near real-time ice-related flood hazard assessment of the exploits river in Newfoundland, Canada. in CGU HS Committee on River Ice Processes and the Environment, 19th Workshop on the Hydraulics of Ice Covered Rivers, Whitehorse, Yukon, Canada. 2017.

[63] Kunz M, Sander J, Kottmeier C. Recent trends of thunderstorm and hailstorm frequency and their relation to atmospheric characteristics in southwest Germany. Int J Climatol 2009;29(15):2283–97.

[64] Eccel E, et al. Quantitative hail monitoring in an alpine area: 35-year climatology and links with atmospheric variables. Int J Climatol 2012;32(4):503–17.

[65] Leslie LM, Leplastrier M, Buckley BW. Estimating future trends in severe hailstorms over the Sydney Basin: a climate modelling study. Atmos Res 2008;87(1):37–51.

[66] Madonna E, Ginsbourger D, Martius O. A Poisson regression approach to model monthly hail occurrence in Northern Switzerland using large-scale environmental variables. Atmos Res 2018;203:261–74.

[67] Yousefi A, Jolaiy S, Hedayati R, Serjouei A, Bodaghi M. Fatigue life improvement of cracked aluminum 6061-T6 plates repaired by composite patches. Materials 2021; 14(6):1421.